

02
Study of stability of heavily boron doped nanodiamond dispersions

© K.M. Kondrina,^{1,2} E.K. Urodkova,³ I.N. Senchikhin,³ S.G. Lyapin,¹ Y.V. Grigoriev,⁴ E.A. Ekimov¹

¹Institute for High Pressure Physics, Russian Academy of Sciences,
108840 Troitsk, Moscow, Russia

²Moscow Institute of Physics and Technology
(National Research University),
141701 Dolgoprudny, Moscow Region, Russia

³Frumkin Institute of Physical Chemistry and Electrochemistry, Russian Academy of Sciences,
119071 Moscow, Russia

⁴ Shubnikov Institute of Crystallography, Kurchatov
Crystallography and Photonics Center, Research and Engineering Center „Kurchatov Institute“,
119333 Moscow, Russia
e-mail: kondrina.km@phystech.edu

Received October 9, 2024

Revised October 9, 2024

Accepted October 9, 2024

Comparative study of water dispersions of boron-doped and detonation nanodiamonds uniformly purified from non-diamond phases in acids reveals high resistance of boron-doped particles to agglomeration and precipitation and its absence in case of detonation nanodiamonds. Boron doped nanodiamonds were obtained by pyrolysis of 9-borabicyclo[3.3.1]nonane dimer $C_{16}H_{30}B_2$ at pressure 8–9 GPa and temperature 1250 °C–1300 °C. The concentration of boron in the synthesized nanodiamonds was estimated using Raman spectroscopy to be at a level of 10^{21} cm^{-3} which corresponds to a heavily doped state. FTIR absorption analysis exposes additional lines in doped diamond spectra characteristic to B–O-groups. The presence of boron on the nanoparticle surface is thought to be responsible for the high stability of the suspension after the acid purification process without the need for additional functionalization. Improved stability of boron-doped nanodiamond in aqueous solutions with a pH of 2.5–8.25 can be a crucial factor for its effective application in electrochemical and biomedical technologies, for seeding of crystallization centers to obtain conducting CVD diamond films without disturbing electrical contact with substrate, and for inkjet printing of patterned boron-doped diamond electrodes.

Keywords: Detonation nanodiamond, High pressures, Oxygen, FTIR, DLS, Electrokinetic potential.

DOI: 10.61011/TP.2025.03.60849.286-24

Introduction

Introduction of the boron admixture into the diamond considerably varies its electrophysical properties. Pure diamond is a semiconductor with a wide irregular prohibited area 5.5 eV, weak doping with boron causes hole conduction with the admixture activation energy 0.37 eV. Stronger doping provides for appearance of metal conductivity under regular temperatures and superconductivity at the liquid helium temperature. Electric transport properties of boron-doped diamonds make it possible to considerably expand the range of diamond practical applications, for example, in electrochemistry for manufacturing of electrodes and sensors. Boron-doped diamond electrodes have high corrosion resistance, stability of properties, a wide potential window (range of low background currents) in the solution of the indifferent electrolyte, critical for electrochemical applications [1,2].

Due to low toxicity and chemical resistance, diamonds find usage in medicine. Nanodiamonds with admixture-vacancy complexes may be used as luminescent biomarkers in delivery of drugs, sensors for measurement of local temperature and magnetic fields. The possibility to use

boron-doped nanodiamonds (BND) in thermotherapy of cancers is reported [3,4], due to effective heating in process of irradiation in the area of skin covering and muscular tissue transparency. Resistance to aggregation of diamond nanoparticles in the wide range of pH and temperatures is a critical factor for using nanodiamonds in biomedicine and other practical spheres.

Colloidal solutions of boron-doped nanodiamonds may be used to apply seeds when depositing the conducting diamond coatings by the CVD method without damage of the electric contact with the substrate [5], to develop liquid supercapacitors [6], and with addition of organic binders — for screen-printing-technologies to produce conducting paths and electrodes [7].

From the richer experience of producing the colloidal solutions based on detonation nanodiamonds (DND) it follows that after cleaning from non-diamond phases, the nanodiamonds have insufficient stability, the suspension particles are not able resist the aggregation for a long period of time. It was established that to produce a stable suspension, it was required to reduce the particle size (< 100 nm) and to modify the surface to increase the force of repulsion between the nanoparticles [8–10].

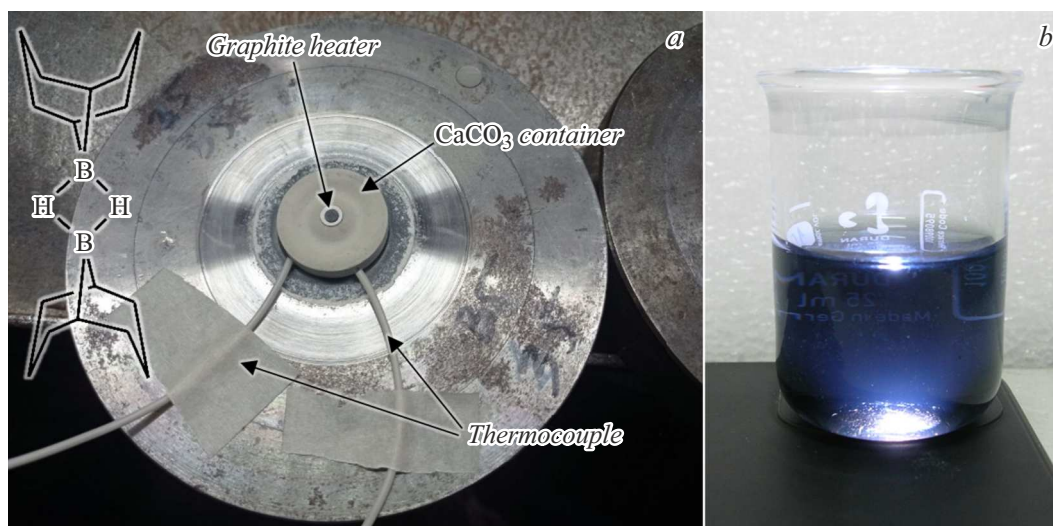


Figure 1. *a* — high pressure chamber with the equipped container and thermocouple, on the insert — structural formula of the initial substance 9-borabicyclo[3.3.1]nonane dimer; *b* — colloidal solution of boron-doped nanodiamonds.

Functionalization of the surface by the treatment in the oxygen-containing atmosphere makes it possible to improve the stability of dispersion of diamond nanoparticles due to formation of oxygen groups on the surface with the negative charge on oxygen. However, the heterogeneity of the detonation nanodiamond surface coating with the functional groups causes their insufficient stability in the practically meaningful solutions [9].

Contrary to the DND, the boron-alloyed nanodiamonds synthesized by the HPHT method, immediately after the acid purification, without additional treatment form the stable colloids [4]. The reasons for formation of stable BND colloids remained unclear, and the impact of such critical factors as pH, temperature and time of existence on the colloidal properties of the solutions — unstudied.

The purpose of this paper was to study the properties of aqueous dispersions of BND and to figure out the nature of nanoparticle stability. The properties of boron-doped nanodiamonds have been studied compared to the properties of detonation nanodiamonds cleaned from non-diamond phases after synthesis in the identical conditions. The effect of temperature on the particle size, the dependence of ξ -potential on pH were studied, and the time dependence of the particle size in the colloidal solution.

1. Experimental part

1.1. Method of synthesis and objects of study

The boron-doped nanodiamonds were produced from an organic precursor, 9-borabicyclo[3.3.1]nonane dimer, $C_{16}H_{30}B_2$ (Sigma Aldrich, 98%), at pressure 8–9 GPa and temperature 1250 °C in accordance with the previously developed synthesis technology [11]. It is assumed that the bridge structure of sp^3 -hybridized carbon frame and

presence of boron in the carbon cycle stimulate the origination and growth of the boron-doped nanodiamonds in process of molecular precursor pyrolysis. To develop high pressures and temperatures, the high-pressure chamber toroid-15 was used (fig. 1). The initial crystalline substance was pressed into pellets with diameter and height of 4 mm, and the pellets were placed into a graphite capsule-heater. The equipped capsule was placed in a container from a lithographic stone (base $CaCO_3$). The heating was done by sending alternating current through the graphite capsule-heater and current leads. Graphite current leads were isolated from an anvil made of solid alloy (WC+Co) using molybdenum discs. Temperature was monitoring using a chromel-alumel thermocouple installed on the outer side of the heater in the middle of its height. The specific soaking time at high pressures and temperatures was 2 min. In certain experiments the synthesis temperature was varied in the interval from 1250 °C to 1400 °C, and synthesis time — from 0.5 to 5 min. The produced specimens were cleaned from non-diamond phases by boiling for around 6 h in a mixture of acids H_2SO_4 and HNO_3 (3:1 by volume). Acid was removed by multiple flushing with distilled water, until diamonds stopped bottoming; pH-of the solution was ≈ 2.5 (fig. 1, *b*). The produced solution has the intensely blue color, the appearance of which is explained by absorption of light caused by admixture of boron in the diamond lattice [5]. As the reference standard, a detonation nanodiamond was chosen in the comparative study of the nanodiamonds we synthesized, the admixture of boron in which is not detected, and the crystal size is 4–5 nm. Since the pre-history of the detonation nanodiamond has significant impact on the chemical condition of its surface [8], the charge with the detonation nanodiamonds was cleaned independently using the unified technology. The charge was produced by detonation of the mix of tritol and hexogen at

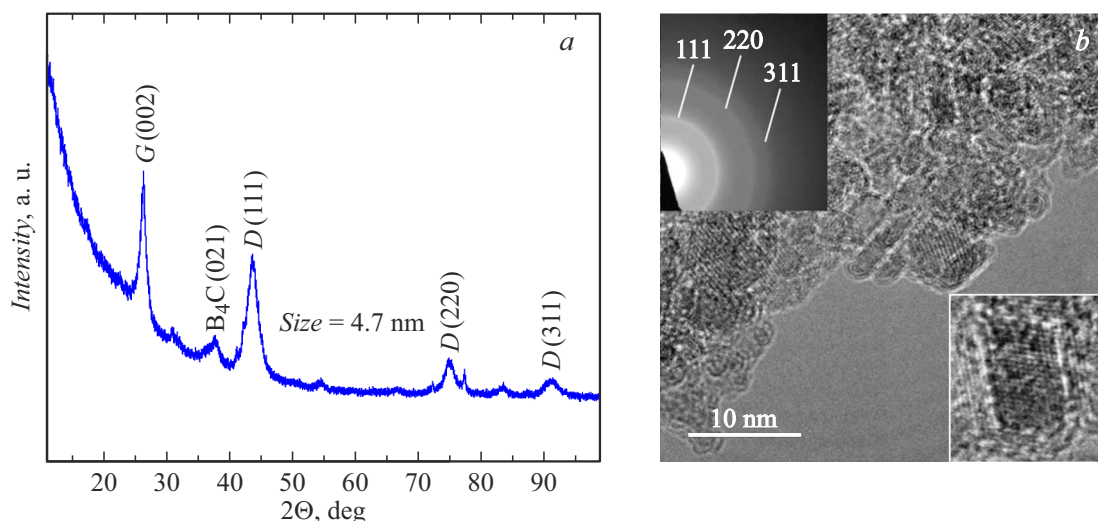


Figure 2. *a* — specific X-ray diffraction pattern of synthesized specimens; *b* — image of the specimen produced using transmission electron microscopy, the insert presents the electron diffraction pattern.

the ratio of 60/40 (Russian Federal Nuclear Center — All Russian Research Institute of Technical Physics, Snezhinsk). Concentration of nanodiamonds in aqueous solutions was around 1 mg/ml.

Ultrasonic treatment of the solution was conducted on Sonoplus ultrasonic homogenizer HD 2070.2 device with a tip of MS 73 3 mm in diameter. The treatment duration was 5 min, the specific capacity was 224 W/cm³.

1.2. Research methods

The average size of nanoparticles in the solution was determined by the dynamic light scattering (DLS) method on Zetasizer Nano ZS device (Malvern, UK), the laser wavelength was 633 nm. The DLS data obtained after the preliminary thermostating of the specimens at 25 °C, were averaged in five serial cycles of measurements, each in its turn being the result of automatic processing of 10–20 „runs“. The results were processed, and the average particle diameter was calculated using software of the device (Zetasizer Software 6.20).

Electrokinetic potential (ξ -potential) was determined at 25 °C using the same device by the method of phase analysis of the scattered light M3-PALS. The results were processed in Zetasizer Software 6.20. The potential value was obtained by averaging of the results in 5 serial cycles of measurements, each in its turn being the result of automatic processing of 100 „runs“.

Diffraction patterns of the synthesized specimens (without washing in acids) were obtained in the „sight-check“ mode using radiation of $\text{CuK}\alpha_1$ on a mylar holder of the specimen (Imaging-plate Guinier camera G670) (Huber).

The experiments with TEM were carried out using a transmission electron microscope of high resolution FEI Tecnai Osiris with a field emission gun that operates on accelerating voltage of 200 kV.

To measure the spectra of infrared (IR) absorption, a drop of colloidal solution of nanodiamonds was applied on the substrate made of ZnSe. IR spectra were measured using Fourier transform infrared spectrometer (FTIR) Bruker Vertex 70, equipped with IR microscope Hyperion 2000, in the spectral range 4000–600 cm⁻¹, with spectral resolution 2 cm⁻¹.

Raman scattering spectra (RSS) were obtained on the cleaned specimens of nanodiamonds at room temperature, to excite the spectra, the 488 nm line of Ar⁺-laser was used. To measure the spectra in the geometry of „back scattering“ spectrometer TriVista 555 was used, equipped with a silicon CCD matrix cooled to the liquid nitrogen temperature. Lens 50x ($NA = 0.50$) of microscope Olympus BX51 was used for laser focusing and signal collection. Spectral width of the slot was less than 3 cm⁻¹. To avoid superheating of the specimens, the laser capacity was less than 0.5 mW.

2. Study results

2.1. Specimen characterization with XPA and TEM methods

The specific diffraction pattern of specimens synthesized at 1250 °C is presented in fig. 2, *a*. The synthesized specimen includes admixture phases of disordered graphite and nanocrystalline boron carbide. The average size of the nanodiamond crystals estimated using Scherrer formula by diamond peak (111) is 4.7 nm. The particle size determined using the XPA data is quite compliant with the thickness of nanocrystals observed in the TEM images (fig. 2, *b*).

2.2. IR spectroscopy

IR absorption spectra were obtained on nanodiamonds after cleaning from the admixture phases in the mixture of

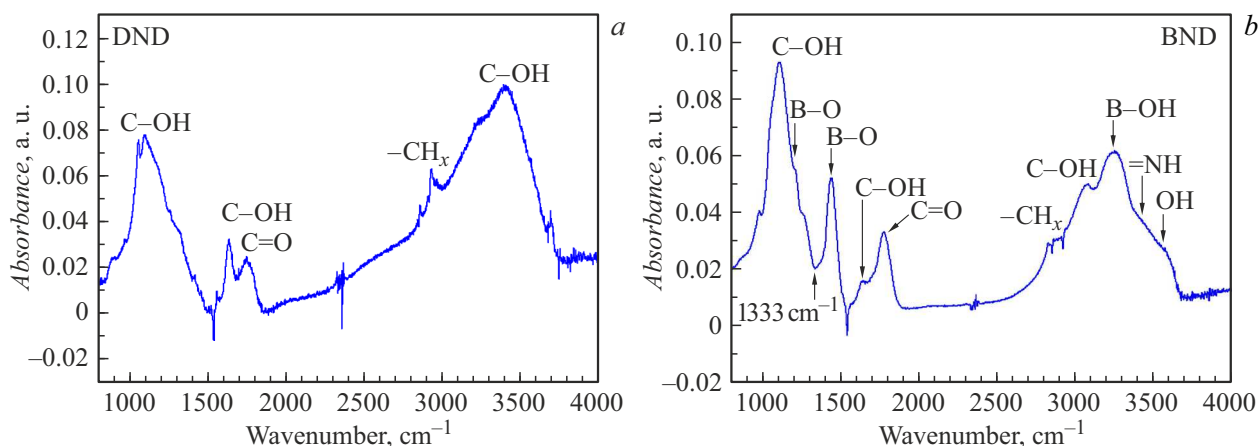


Figure 3. IR absorption spectra for: *a* — DND, *b* — BND.

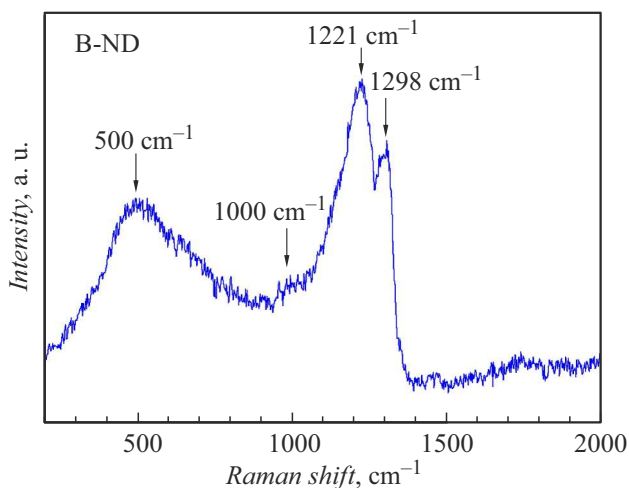


Figure 4. RSS spectrum of the boron-doped nanodiamonds after cleaning in acids, where peaks are present that are specific for boron admixture.

acids. Both for DND and BND (fig. 3) the IR spectra show the presence of the lines specific for diamonds with the oxidized surface.

The following features are common for two spectra — wide peak at $1000\text{--}1500\text{ cm}^{-1}$, which may correspond to the valent oscillation C–O–C, or deformation oscillation O–H [12]. The nature of the peak near 1630 cm^{-1} is related to the deformation mode O–H, and the nature of the peak at 1750 cm^{-1} — to the valent oscillation of C = O-group [13]. The feature at 2200 cm^{-1} is related not to the specimen, but to the atmospheric CO_2 , and in the area of 3000 cm^{-1} it is also connected to either the background from ZnSe, or to the valent oscillations $-\text{CH}_x$ [12]. The last wide peak at $3000\text{--}3700\text{ cm}^{-1}$ is related to valent $-\text{OH}$ -oscillations [12,14].

For BND the features related to boron are found: covalent bond B–O produces absorption peaks 3200 cm^{-1} (valent oscillations B–OH), $1195, 1440\text{ cm}^{-1}$ [15,16].

A dip in the IR-spectrum of BND at frequencies of around 1333 cm^{-1} may presumably be related to the Fano resonance of the diamond Raman mode with the continuum of conducting surface states [17]. Besides, the Fano resonance was observed in IR spectra of boron-doped diamonds produced by CVD method [18].

2.3. RSS spectroscopy

RSS spectrum of the crystals after cleaning in acids (fig. 4) confidently demonstrates entrance of boron into the lattice: the spectra include peaks of $500, 1000, 1220, 1300\text{ cm}^{-1}$, specific for diamonds highly doped with boron [19,20]. Contrary to the spectra of the nanodiamonds synthesized from halogenated hydrocarbons under pressure [21], the spectra show no peaks related to oscillations of bonds C–H. There are no peaks of sp^2 carbon *D* and *G*, specific for detonation nanodiamonds [14]. Shift and broadening of the phonon peak in the center of the Brillouin zone 1330 cm^{-1} make it possible to estimate the boron concentration at the level of $3 \cdot 10^{21}\text{ cm}^{-3}$ [22,23].

2.4. DLS measurements

Fig. 5, *a* presents a DLS spectrum for BND, after washing with acids and ultrasonic treatment, compared to DND processed in the same manner with particle concentration of 1 mg/ml . The data is provided for the distribution of the particle number, and the intensity distribution, which is proportionate to the number of particles and size of particles of degree six, and may therefore provide information on the presence of large particle fraction. To compare the particle size, the curves specify the parameter of average hydrodynamic diameter of particles (indicated as Z-average size). For nanodiamonds with the average crystal size of 4 nm , estimated from the X-ray diffraction data, the average size of BND particles using the DLS data was 29 nm . The determination of the larger particle size in DLS may be due to aggregation of particles, presence of a solvate shell or

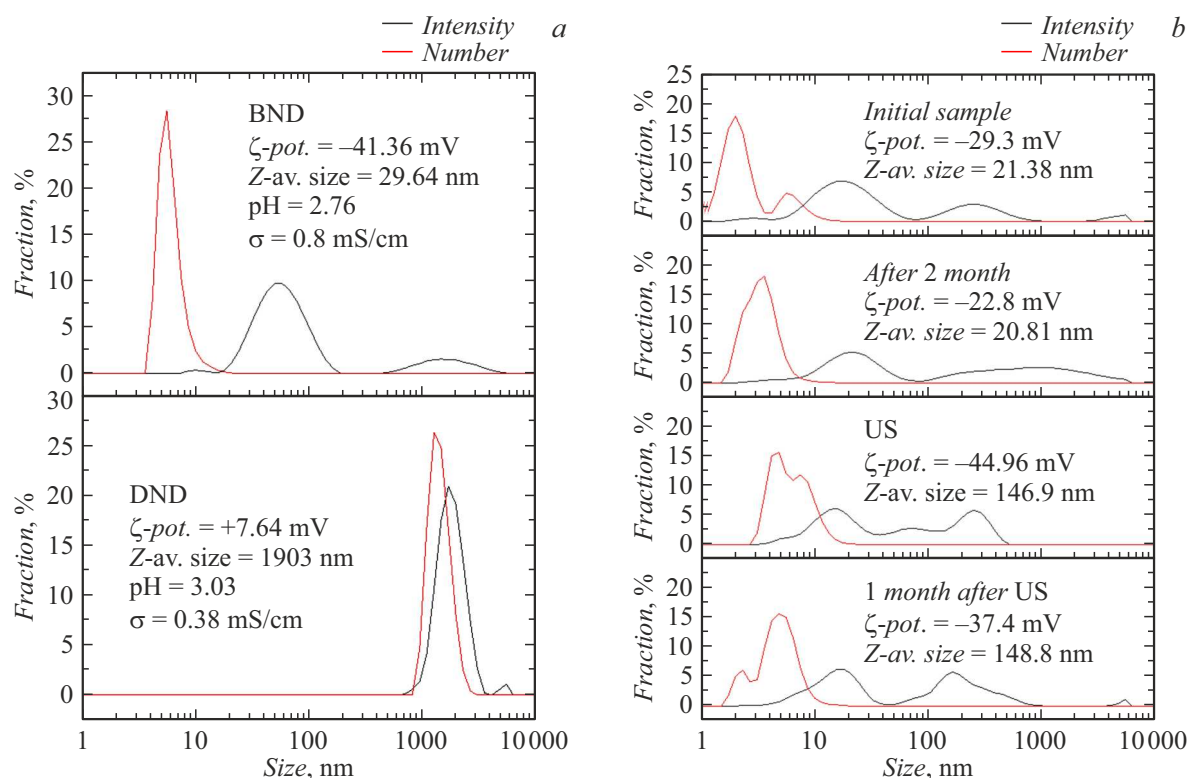


Figure 5. BND DLS distributions: *a* — comparison to DND, *b* — time dependence and ultrasonic treatment.

particle polycrystallinity. The size distribution by intensity is not monomodal — there are fractions of large aggregated particles present that exceed 100 nm. For DND the average size determined in DLS is much larger, and the particles bottom fast. Contrary to the BND, acid treatment of DND in process of cleaning from non-diamond phases does not result in stable colloidal solutions. pH measurements for all specimens show the presence of acid residues, which may not be fully removed by cleaning in the distilled water, and the large value of conductivity of 10^{-3} S/cm order seems to be related to the presence of the acid residues.

Electrokinetic potential makes it possible to quantitatively determine the stability of the colloid — the solution is deemed stable if ζ -potential is higher than 30 mV by absolute value [24,25].

Therefore, potential of -40 mV indicates the stability of the BND solution, and the same treatment with acids did not make it possible to produce a stable solution of detonation nanodiamond.

Fig. 5, *b* presents the dependence of the BND colloidal solution stability immediately after production, two months after production, also immediately after ultrasonic treatment and in a month after treatment. Ultrasonic treatment makes it possible to increase the electrokinetic potential, but the aggregated particles may be broken only partially — the peak of more than 100 nm is maintained. And the average size after the ultrasonic treatment increased. In one month the electrokinetic potential reduced by 5 mV by absolute

value, but it is still more than 30 mV; the large particle peak increased more than 100 nm, but no precipitation takes place. Therefore, the experiment data support the colloidal system stability in time.

Fig. 6, *a* presents the change of the electrokinetic potential and particle size at pH variation. The system stability is observed in the pH 2.5–8 area, which is necessary for medical applications.

Fig. 6, *b* shows the impact of temperature in the range of 25 °C–40 °C. The curves show that the temperature rise results in decrease of the Z-average size determined by intensity, but the average size determined by particle number increases at 25 °C–35 °C. All changes in the particle size vary within 10 %, we do not see the rapid growth of their hydrodynamic diameter, and no precipitation occurs. Therefore, the DLS method does not demonstrate the aggregation of the particles with the temperature rise in the studied interval, indicating temperature stability of the colloidal system based on BND in the temperature range critical for the biological application.

A common drawback that restricts medical application of colloidal nanodiamonds is the aggregation of nanoparticles. Indeed, we can see a fraction of large particles of more than 100 nm in all DLS experiments. And the ultrasonic treatment does not eliminate this fraction. [26] proposed the method to separate the particles using centrifuging. In this paper the treatment of colloidal solutions based on BND in the centrifuge was carried out for 3 h at acceleration of

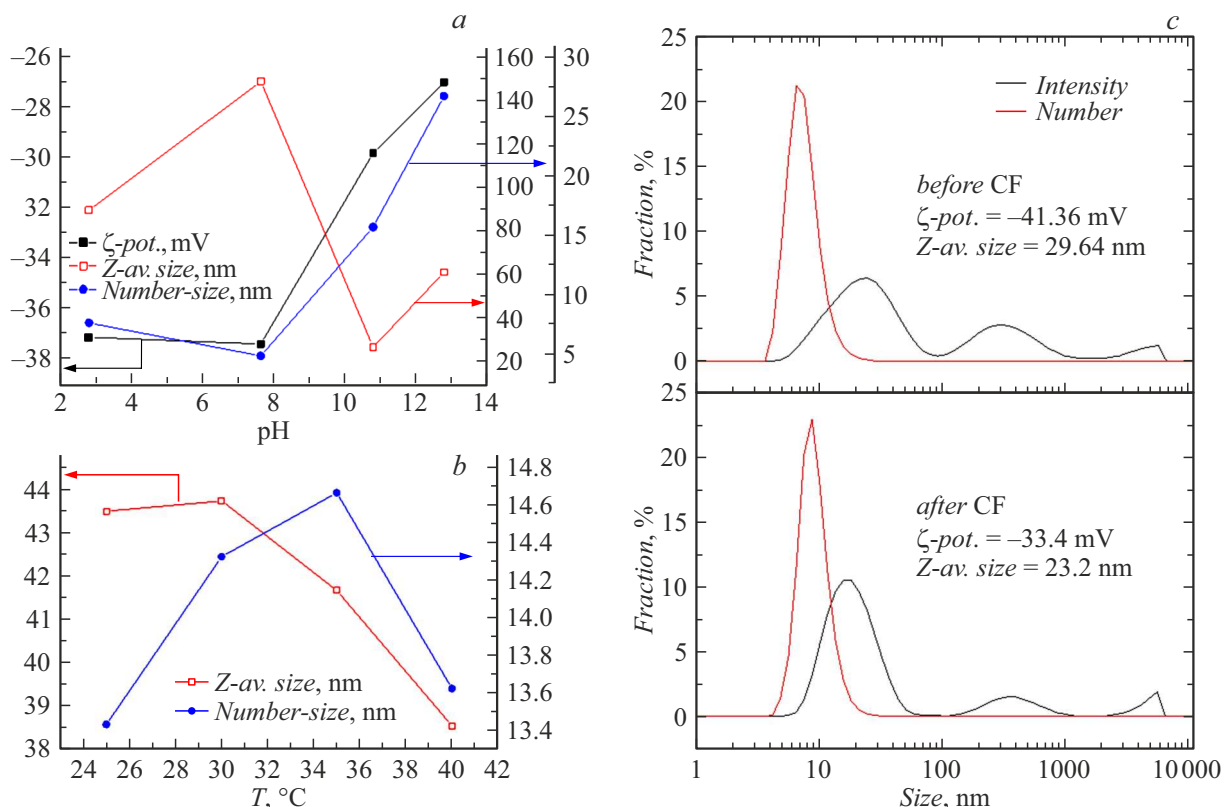


Figure 6. *a* — dependence of size and electrokinetic potential of BND on pH, *b* — dependence of particle size on temperature, *c* — comparison of specimen DLS before and after treatment in the centrifuge.

27530 g. Fig. 6, *c* provides the DLS spectra before and after centrifuging, from which it follows that such treatment may not fully remove the large particles, even though the size ratio changed, and the distribution of intensity for the most intense peak shifted to the area of smaller size.

Apart from the centrifuging method, there are other methods to control the particle size, for example, annealing in the oxygen atmosphere [27]. In case of HPHT synthesis from 9BBN the crystal size may be controlled by changing the synthesis parameters, namely the synthesis time temperature. Therefore, this method makes it possible to compare the stability of colloids for various sizes of nanodiamond crystals.

To produce the crystals of various dimensions, the following synthesis parameters were changed — temperature and soaking time. The specimens with the nanocrystal sizes of 3.2, 4.0 and 4.7 nm were obtained at temperature 1250 °C, for the soaking time of accordingly 0.5, 2 and 5 min. The specimen with the crystal size of 7.3 nm was obtained at 1300 °C for the synthesis time of 2 min. The specimen with the crystal size of 28 nm was obtained at 1400 °C, the synthesis time was 2 min. The crystal size was estimated using the Scherrer's formula for broadening of the X-ray diffraction peak (111) of the diamond, the XPA data are presented in fig. 7, *a*.

Fig. 7, *b* presents the DLS data for colloidal solutions produced using nanodiamonds with different crystal size.

The curves also note the maximum distribution of the particle number, which makes it possible to track the change in the fraction size of small particles.

Fig. 7, *c* presents the data on the stability of colloidal dispersions with different nanoparticle size. The stability was compared depending on the size, at the ζ -potential value is above 30 mV by absolute value for nanoparticles with the dimensions in the range of 3.2–7.3 nm, which corresponds to the colloidal stability. Size increase to 28 nm produces an unstable solution.

3. Discussion of the system stability

From the previous experience of producing colloidal solutions based on DND it follows that their stability depends on some factors, the main being the functionalization of the diamond surface. The oxidized surface is hydrophilic, and may form a colloid due to the presents of the partial negative charge on the oxygen. Besides, the stability also depends on the method of surface oxidation, since depending on the treatment, various oxygen-containing groups may be formed [8,28]. The nanodiamond surface also often contains sp^2 -carbon chains, they provide another explanation of the conductance in the hydrogenated nanodiamonds, which may also form colloids [17,29].

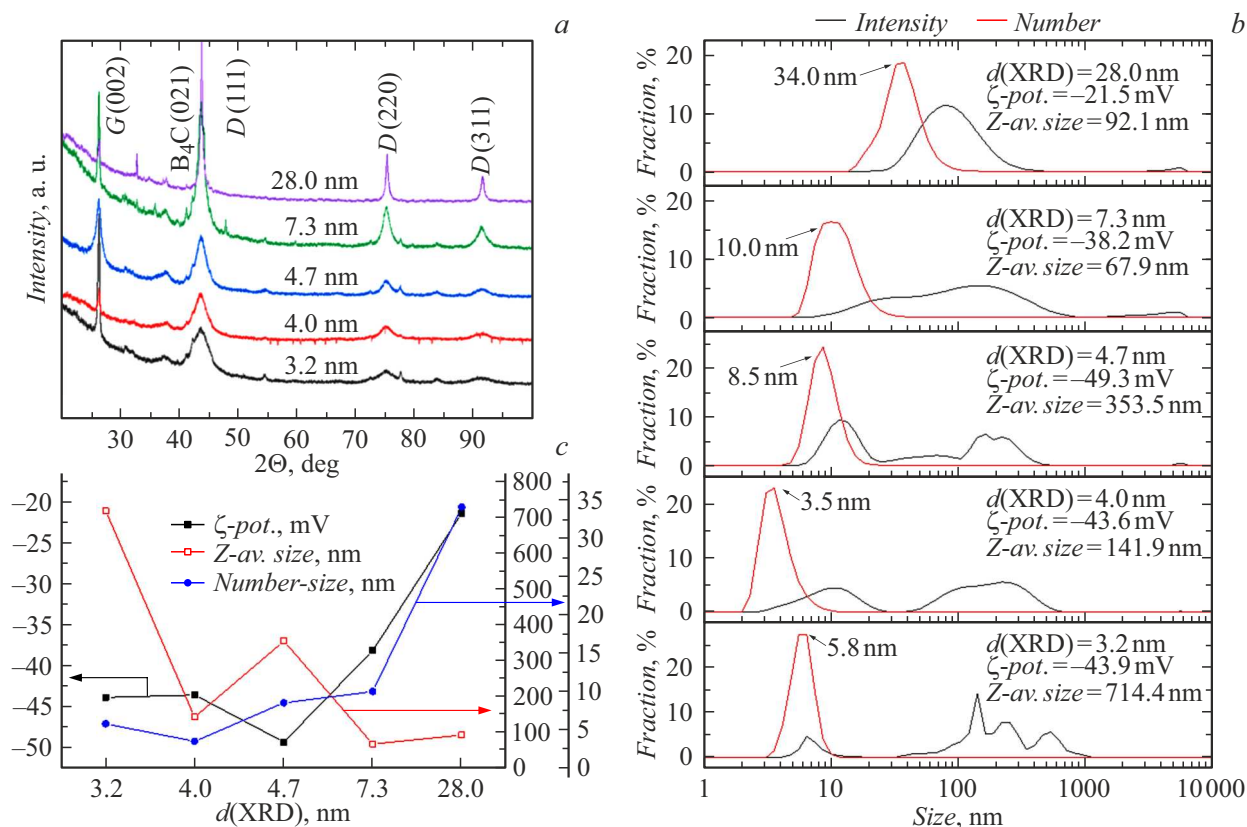


Figure 7. *a* — XPA data of BND specimens with different diameter, *b* — DLS, *c* — comparison of properties for difference sizes of nanoparticles.

In our paper the electrokinetic potential of BND particles is negative, first of all it may be related to formation of $-\text{COOH}$ -, $-\text{OH}$ -, $=\text{O}$ -groups on the diamond surface when washed with acid [8].

However, this method of surface treatment did not result in formation of a stable colloid for a detonation nanodiamond, its electrokinetic potential is positive and equal to $+7.64$ mV. This result matches the results published in paper [28], which compared different methods of DND washing, and use of mixture $\text{H}_2\text{SO}_4:\text{HNO}_3$ provided for low stability. IR spectra of DND show no $-\text{CH}$ -groups, therefore the positive ζ -potential of DND may be related to the presence of unsaturated groups on the surface — quinones, pyrones, or conjugate sp^2 -carbon chains [8].

Therefore, comparison to the detonation diamond treated by the same method detects the impact of boron admixtures at zeta-potential. The theoretical papers demonstrated that boron admixtures should stay near the surface [30,31], besides, they had a charge, a positive or a negative one depending on their location — the charge is affected by the closeness to the surface and its crystal-lattice orientation. In our specimens the boron content was determined at the level of $3 \cdot 10^{21} \text{ cm}^{-3}$, which corresponds to approximately every 50-th atom.

The boron on the surface may interact with the water molecules, water may be adsorbed on the boron admixture

using donor-acceptor mechanism to form a bond B—O, visible in IR spectra (fig. 3, *b*). It was shown that the formation of such group would reinforce the interaction with the water molecules using hydrogen bonds, therefore the surface will become more hydrophilic [32]. The impact of the boron admixtures on the surface was detected experimentally for silicon nanoparticles — the change in the particle conductance was shown as a result of adsorption of the larger number of water molecules on bond B—O [33].

It is interesting that interaction of the diamond surface with water also bends the crystal zones. If there is oxygen on the surface, it creates a surface layer that is the donor [34]. This level is distanced from the valence band by 1.7 eV, and in the crystal volume the distance to the Fermi level is 0.9 eV — this difference causes upward bending of the zones, and the layer with excess of electrons is formed under the surface. And the energy difference increases additionally for the nanodiamond [14]. The boron-doped oxidized diamond may also demonstrate an upward bend of the zones, which causes appearance of the depleted hole layer, also reinforcing the hydrophilic nature of the surface [35]. However, in this paper we are not able to estimate how strongly this effect will impact the colloid stability.

Therefore, appearance of BND nanoparticle high resistance to aggregation in the aqueous solution may not be

explained only by acid treatment. The large quantity of boron on the surface improves the hydrophilic properties.

The interesting continuation of this paper may be the study of impact from hydrogen saturation of the boron-doped nanodiamonds. It would be interesting to test whether in this case it is possible to form a stable colloidal solution of boron-doped nanodiamond, or the listed effects will prevent stabilization of the hydrogenated particles.

Conclusion

It is shown that it is possible to produce a colloidal solution of boron-doped nanodiamonds, differing with high aggregative stability, determined using the electrokinetic potential measurements. We explain the high stability by not only the presence of $-\text{COOH}$ -, $-\text{OH}$ -, $=\text{O}$ -groups on the surface due to acid treatment, but also by presence of the boron admixture, the concentration of which was determined using the DLS spectra and was $3 \cdot 10^{21} \text{ cm}^{-3}$. The boron admixture is also located on the surface, which manifests itself in forming B–O bond found in the IR absorption spectra. In accordance with the literature data, the presence of such group improves the surface hydrophilic behavior and better solution stability. Our experiments to study the properties of this system show that it remains stable at pH variation in the range of 2.5–8, and the temperature change in the interval of 25°C – 40°C has no effect on the particle size and does not cause their aggregation. The comparison was done on the stability of the systems with different particle size, the particle stability is shown with the sizes in the range of 3.2–7.3 nm.

Acknowledgments

The DLS spectra measurement experiments were supported by the Ministry of Science and Higher Education of the Russian Federation. The work was performed using the equipment of the Collective Use Center of Frumkin Physical Chemistry and Electrochemistry Institute of the Russian Academy of Sciences.

Funding

The study was performed with the support of the Russian Science Foundation grant № 24-12-00037, <https://rscf.ru/en/project/24-12-00037/>.

Conflict of interest

The authors declare that they have no conflict of interest.

References

- [1] K. Muzyka, J. Sun, T.H. Fereja, Y. Lan, W. Zhang, G. Xu. *Anal. Methods*, **11** (4), 397 (2019). DOI: 10.1039/C8AY02197J
- [2] Z. Liu, S. Baluchová, B. Brocken, E. Ahmed, P. Pobedinskas, K. Haenen, J.G. Buijnsters. *ACS Appl. Mater. Interfaces*, **15** (33), 39915 (2023). DOI: 10.1021/acscami.3c04824
- [3] J.X. Qin, X.G. Yang, C.F. Lv, Y.Z. Li, K.K. Liu, J.H. Zang, X. Yang, L. Dong, C.X. Shan. *Mater. Des.*, **210**, 110091 (2021). DOI: 10.1016/j.matdes.2021.110091
- [4] A.M. Verval, S.A. Burikov, A.M. Scherbakov, O.S. Kudryavtsev, N.A. Kalyagina, I.I. Vlasov, E.A. Ekimov, T.A. Dolenko. *ACS Biomater. Sci. Eng.*, **6** (8), 4446 (2020). DOI: 10.1021/acsbio.0c00505
- [5] S. Heyer, W. Janssen, S. Turner, Y.G. Lu, W.S. Yeap, J. Verbeeck, K. Haenen, A. Krueger. *ACS Nano*, **8** (6), 5757 (2014). DOI: 10.1021/nn500573x
- [6] T. Kondo, T. Kato, K. Miyashita, T. Aikawa, T. Tojo, M. Yuasa. *J. Electrochem. Soc.*, **166** (8), A1425, (2019). DOI: 10.1149/2.0381908jes
- [7] T. Kondo. *Chem. Lett.*, **50** (4), 733 (2021). DOI: 10.1016/j.colelec.2021.100891
- [8] N. Gibson, O. Shenderova, T.J.M. Luo, S. Moseenkov, V. Bondar, A. Puzyr, K. Purto, Z. Fitzgerald, D.W. Brenner. *Diamond Relat. Mater.*, **18** (4), 620 (2009). DOI: 10.1016/j.diamond.2008.10.049
- [9] C. Bradac, I.D. Rastogi, N.M. Cordina, A. Garcia-Bennett, L. Brown. *J. Diamond Relat. Mater.*, **83**, 38 (2018). DOI: 10.1016/j.diamond.2018.01.022
- [10] A.T. Dideikin, A.E. Aleksenskii, M.V. Baidakova, P.N. Brunkov, M. Brzhezinskaya, V.Y. Davydov, V.S. Levitskii, S.V. Kidalov, Yu.A. Kukushkina, D.A. Kirilenko, V.V. Shnitov, A.V. Shvidchenko, B.V. Senkovskiy, M.S. Shestakov, A.Y. Vul. *Carbon*, **122**, 737 (2017). DOI: 10.1016/j.carbon.2017.07.013
- [11] E.A. Ekimov, O.S. Kudryavtsev, S. Turner, S. Korneychuk, V.P. Sirotinkin, T.A. Dolenko, A.M. Verval, I.I. Vlasov. *Phys. Status Solidi (A)*, **213** (10), 2582 (2016). DOI: 10.1002/pssa.201600181
- [12] S. Stehlik, T. Glatzel, V. Pichot, R. Pawlak, E. Meyer, D. Spitzer, B. Rezek. *Diamond Relat. Mater.*, **63**, 97 (2016). DOI: 10.1016/j.diamond.2015.08.016
- [13] O. Shenderova, A.M. Panich, S. Moseenkov, S.C. Hens, V. Kuznetsov, H.M. Vieth. *J. Phys. Chem. C*, **115** (39), 19005 (2011). DOI: 10.1021/jp205389m
- [14] D. Miliáieva, A.S. Djoumessi, J. Čermák, K. Kolářová, M. Schaal, F. Otto, E. Shagieva, O. Romanyuk, J. Jiří Pangrác, J. Kulček, V. Nádaždy, S. Stehlik, A. Kromka, H. Hoppe, B. Rezek. *Nanoscale Adv.*, **5** (17), 4402 (2023). DOI: 10.1039/D3NA00205E
- [15] Y. Andriani, J. Song, P.C. Lim, D.H.L. Seng, D.M.Y. Lai, S.L. Teo, J. Kong, X. Wang, X. Zhang, S. Liu. *Ceram. Int.*, **45** (4), 4909 (2019). DOI: 10.1016/j.ceramint.2018.11.190
- [16] M.N. Mirzayev. *Int. J. Mod. Phys. B*, **34** (18), 2050160 (2020). DOI: 10.1142/S021797922050160X
- [17] E. Ekimov, A.A. Shiryaev, Y. Grigoriev, A. Averin, E. Shagieva, S. Stehlik, M. Kondrin. *Nanomater.*, **12** (3), 351 (2022). DOI: 10.3390/nano12030351
- [18] J.W. Ager III, W. Walukiewicz, M. McCluskey, M.A. Plano, M.I. Landstrass. *Appl. Phys. Lett.*, **66** (5), 616 (1995). DOI: 10.1063/1.114031
- [19] F. Pruvost, E. Bustarret, A. Deneuille. *Diamond Relat. Mater.*, **9** (3-6), 295 (2000). DOI: 10.1016/S0925-9635(99)00241-1
- [20] V. Mortet, A. Taylor, Z.V. Živcová, D. Machon, O. Frank, P. Hubík, D. Tremouilles, L. Kavan. *Diamond Relat. Mater.*, **88**, 163 (2018). DOI: 10.1016/j.diamond.2018.07.013

- [21] E.A. Ekimov, S.G. Lyapin, Y.V. Grigoriev, I.P. Zibrov, K.M. Kondrina. *Carbon*, **150**, 436 (2019). DOI: 10.1016/j.carbon.2019.05.047
- [22] V. Mortet, Z.V. Živcová, A. Taylor, M. Davydová, O. Frank, P. Hubík, J. Lorincik, M. Aleshin. *Diamond Relat. Mater.*, **93**, 54 (2019). DOI: 10.1016/j.diamond.2019.01.028
- [23] *Raman Analysis Tool*. <https://ramantool.pythonanywhere.com/>
- [24] T.M. Riddick. *Zeta-Meter Operating Manual zm-75* (Zeta-Meter, Inc., NY., 1968)
- [25] J.D. Clogston, A.K. Patri. *Zeta Potential Measurement*. In: *Characterization of Nanoparticles Intended for Drug Delivery. Methods in Molecular Biology*, ed. by E. Scott, McNeil (New Jersey, Humana Press, 2011), v. 697, p. 63–70. DOI: 10.1007/978-1-60327-198-1_6
- [26] S. Stehlik, M. Varga, M. Ledinsky, V. Jirasek, A. Artemenko, H. Kozak, L. Ondic, V. Skakalova, G. Argentero, T. Pennycook, J.C. Meyer, A. Fejfar, A. Kromka, B. Rezek. *J. Phys. Chem. C*, **119** (49), 27708 (2015). DOI: 10.1021/acs.jpcc.5b05259
- [27] S. Stehlik, M. Varga, M. Ledinsky, D. Miliaieva, H. Kozak, V. Skakalova, C. Mangler, T.J. Pennycook, J.C. Meyer, A. Kromka, B. Rezek. *Sci. Rep.*, **6** (1), 38419 (2016). DOI: 10.1038/srep38419
- [28] A.P. Koshcheev. *Russ. J. General Chem.*, **79** (9), 2033 (2009). DOI: 10.1134/S1070363209090357
- [29] T. Petit, H.A. Girard, A. Trouvé, I. Batonneau-Gener, P. Bergonzo, J.C. Arnault. *Nanoscale*, **5** (19), 8958 (2013). DOI: 10.1039/C3NR02492J
- [30] A.S. Barnard, M. Sternberg. *Diamond Relat. Mater.*, **16** (12), 2078 (2007). DOI: 10.1016/j.diamond.2007.05.011
- [31] A.S. Barnard, M. Sternberg. *J. Phys. Chem. B*, **110** (39), 19307 (2006). DOI: 10.1021/jp0634252
- [32] C.A. Latorre, J.P. Ewen, D. Dini, M.C. Righi. *Carbon*, **171**, 575 (2021). DOI: 10.1016/j.carbon.2020.09.044
- [33] M. Sasaki, S. Kano, H. Sugimoto, K. Imakita, M. Fujii. *J. Phys. Chem. C*, **120** (1), 195 (2016). DOI: 10.1021/acs.jpcc.5b05604
- [34] J. Shirafuji, T. Sugino. *Diamond Relat. Mater.*, **5** (6-8), 706 (1996). DOI: 10.1016/0925-9635(95)00415-7
- [35] Z. Futera, T. Watanabe, Y. Einaga, Y. Tateyama. *J. Phys. Chem. C*, **118** (38), 22040 (2014). DOI: 10.1021/jp506046m

Translated by M.Verenikina